Acta Crystallographica Section D
Biological Crystallography
ISSN 1399-0047

Structure of crenactin, an archaeal actin homologue active at 90°C

Ann-Christin Lindås,[a] Maksymilian Chruszcz,[b] Rolf Bernander[a]* and Karin Valegård[c]

[a]Department of Molecular Biosciences, The Wenner-Gren Institute, Stockholm University, Stockholm, Sweden, [b]Department of Chemistry and Biochemistry, University of South Carolina, Columbia, South Carolina, USA, and [c]Department of Cell and Molecular Biology, Uppsala University, Uppsala, Sweden

Correspondence e-mail: rolf.bernander@su.se

Received 27 November 2013
Accepted 14 January 2014

PDB reference: crenactin, 4bql

The crystal structure of the archaeal actin, crenactin, from the rod-shaped hyperthermophilic (optimal growth at 90°C) crenarchaeon *Pyrobaculum calidifontis* is reported at 3.35 Å resolution. Despite low amino-acid sequence identity, the three-dimensional structure of the protein monomer is highly similar to those of eukaryotic actin and the bacterial MreB protein. Crenactin-specific features are also evident, as well as elements that are shared between crenactin and eukaryotic actin but are not found in MreB. In the crystal, crenactin monomers form right-handed helices, demonstrating that the protein is capable of forming filament-like structures. Monomer interactions in the helix, as well as interactions between crenactin and ADP in the nucleotide-binding pocket, are resolved at the atomic level and compared with those of actin and MreB. The results provide insights into the structural and functional properties of a heat-stable archaeal actin and contribute to the understanding of the evolution of actin-family proteins in the three domains of life.

1. Introduction

Actin is a hallmark of the eukaryotic cell. Proteins belonging to the actin family are among the most abundant and well conserved, and are involved in a wide range of structural functions and force-dependent activities, ranging from cell-shape modulation and motility to phagocytosis and cytokinesis (van den Ent *et al.*, 2001; Carballido-López, 2006; Pollard & Cooper, 2009).

Actin monomers (G-actin) polymerize into polar filaments (F-actin) that consist of a helical structure with two parallel polymers twisted around each other (Holmes *et al.*, 1990; Fujii *et al.*, 2010). ATP is an essential cofactor for filament formation and contributes to stabilization of the polymer (Kabsch *et al.*, 1990). The filaments grow by the addition of ATP-bound monomers, mainly at the (+)-end. The nucleotide is hydrolyzed to ADP within the filament, releasing the γ-phosphate, and ADP-bound G-actin is eventually released from the (−)-end during filament turnover.

Multiple subfamilies of actin-related proteins (ARPs), which display moderate similarity to actin, have also been identified (Schafer & Schroer, 1999; dos Remedios *et al.*, 2003). ARPs play important roles, for example, in chromatin-remodelling processes in the nucleus, as components of the cytoskeleton and in dynein-mediated vesicle transport. Furthermore, several hundred actin-binding proteins (ABPs) interact with different protein motifs both in actin monomers and filaments, thereby modulating actin-polymerization rates, the intracellular localization of actin polymers and the structural and functional properties of different actin-filament variants (Goodson & Hawse, 2002; Vorobiev *et al.*, 2003).

In addition to the various eukaryotic variants, the actin superfamily also encompasses members from both the bacterial and archaeal domains of life. Bacterial actin-like proteins include ParM plasmid partitioning proteins (van den Ent *et al.*, 2002), MamK proteins involved in magnetosome organization (Komeili *et al.*, 2006), Hsp70 heat-shock proteins (Bork *et al.*, 1992) and a divergent family of actin-like proteins (ALPs) of largely unknown function (Derman *et al.*, 2009). MreB proteins are also prominent members of the bacterial actin family and have been shown to form spiral-shaped intracellular structures that play a key role in cell-shape determination (van der Ent *et al.*, 2001; Jones *et al.*, 2001).

Within the archaeal domain, species belonging to the order Thermoplasmatales within the phylum Euryarchaeota have been shown to contain a ParM-like protein, which consequently has been suggested to function in plasmid partitioning (Roeben *et al.*, 2006). Furthermore, MreB homologues are found in several methanogen lineages (also in the phylum Euryarchaeota), including the genera *Methanothermobacter*, *Methanobrevibacter* and *Methanopyrus* (Jones *et al.*, 2001). These MreB homologues, which may have been introduced through horizontal transfer from bacteria (Yutin *et al.*, 2009), may be involved in shape determination since elongated cell morphologies are evident in all three genera, although functional studies have not been reported.

Archaea belonging to the order Thermoproteales within the phylum Crenarchaeota also encode an actin-family protein (Yutin *et al.*, 2009), crenactin (Ettema *et al.*, 2011), which

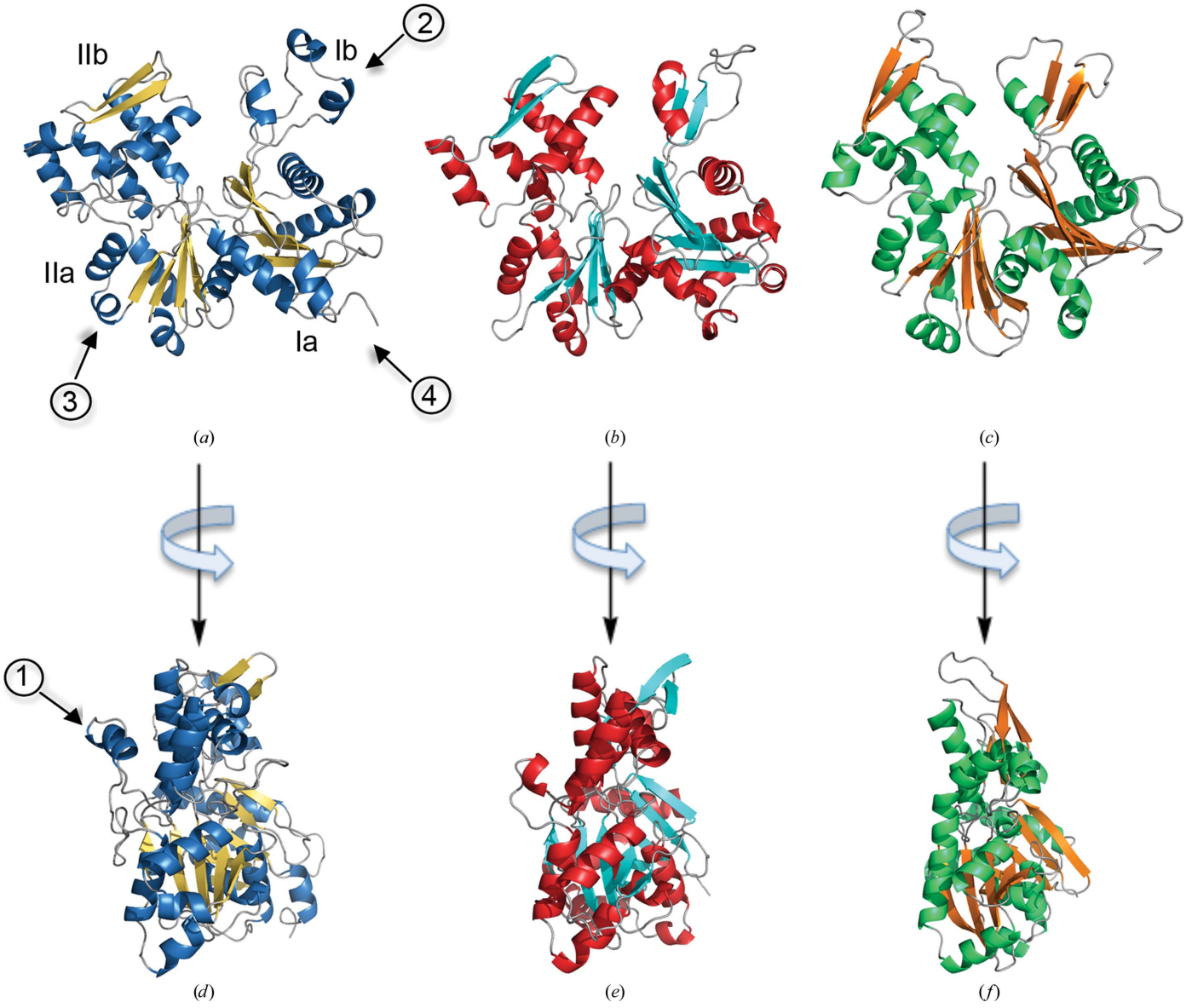

Figure 1
Comparison of monomer structures of (*a*) crenactin from *P. calidifontis* in the ADP form, (*b*) yeast actin from *S. cerevisiae* in the ATP form (PDB entry 1yag; Vorobiev *et al.*, 2003) and (*c*) MreB from *T. maritima* in complex with AMP-PNP (PDB entry 1jcg; van den Ent *et al.*, 2001). The characteristic Ia, Ib, IIa and IIb subdomains of actin-family proteins are indicated in the *P. calidifontis* structure. (*d*), (*e*) and (*f*) show the views generated after a 90° rotation along the vertical axis of the structures in (*a*), (*b*) and (*c*), respectively. Four major differences between crenactin and the other two actin-family members are indicated by arrows and numbers. The differences are also indicated in the structure-based sequence alignment in Fig. 2.

affiliates closely with eukaryotic homologues in phylogenetic analyses, while MreB and other prokaryotic actin-family members are significantly more distantly related (Carballido-López, 2006). Despite its similarity to eukaryotic counterparts, crenactin from the hyperthermophilic archaeon *Pyrobaculum calidifontis* (Amo *et al.*, 2002) has been shown to form spiral-shaped structures that span the cell from pole to pole (Ettema *et al.*, 2011), similar to structures observed for MreB (van den

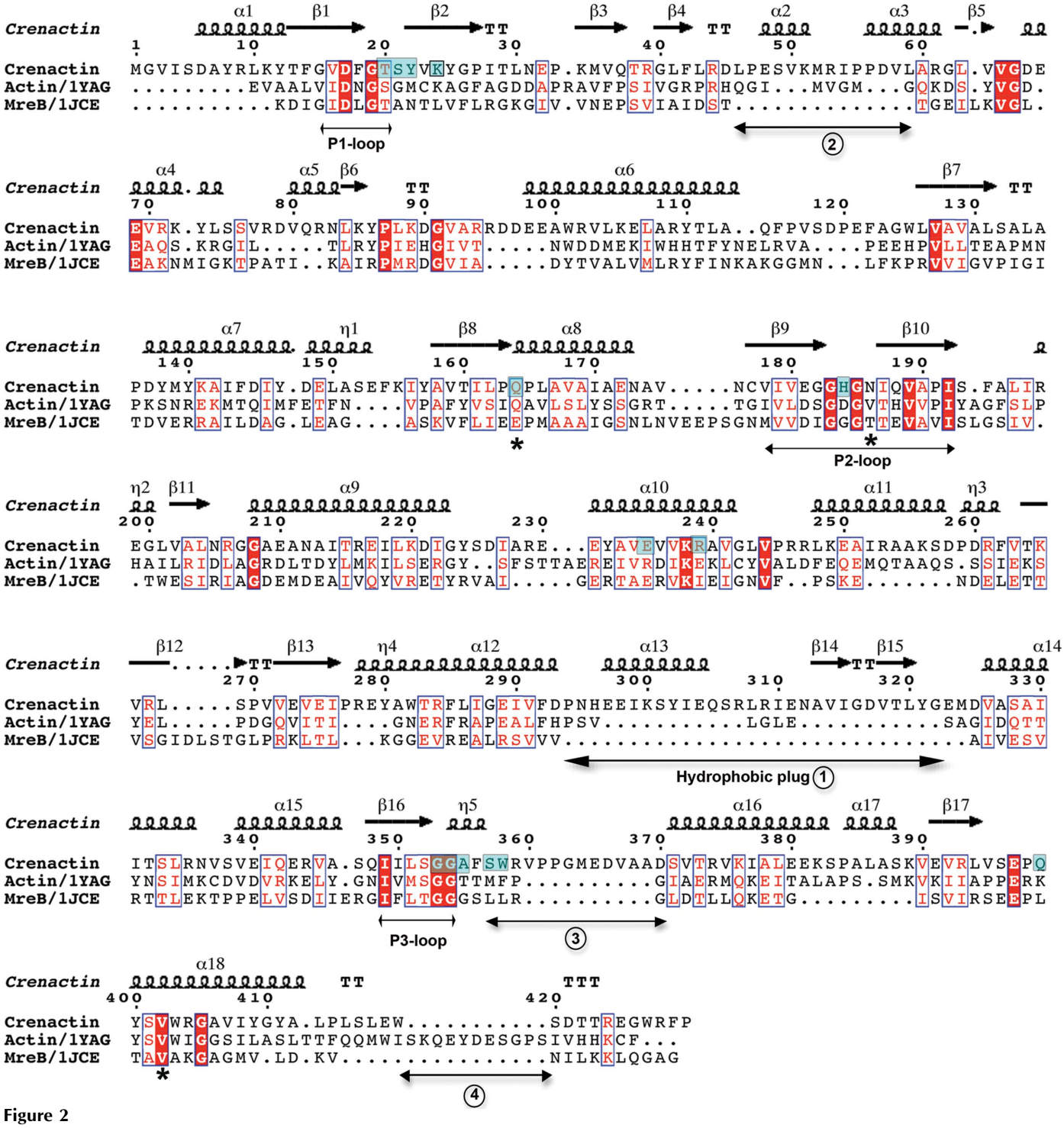

Figure 2
Structure-based sequence alignment between crenactin, eukaryotic actin and bacterial MreB. The alignment is based on a three-dimensional comparison between crenactin from *P. calidifontis*, yeast actin from *S. cerevisiae* (PDB entry 1yag) and MreB from *T. maritima* (PDB entry 1jcg) using the *DALI* web server (Holm & Rosenström, 2010). The three highly conserved P-loops are indicated, as are the hydrophobic plug in eukaryotic actin and the major differences between crenactin and the other actin-family members (1–4; see Fig. 1). Homologous regions are boxed, with identical amino-acid residues indicated as bold white letters on a red background and functionally equivalent residues indicated as red letters. Amino-acid residues that interact with ADP are shown on a cyan background. The three residues involved in the recognition of the antibiotic A22 in MreB are indicated by asterisks (*). Secondary-structure elements and numbering for crenactin are indicated above the sequences: spirals, α-helices; arrows, β-sheets; T, turns.

Table 1
Data-collection and refinement statistics for SeMet crenactin.

Values in parentheses are for the outer resolution shell.

PDB code	4bql
X-ray source	ID29, ESRF
Wavelength (Å)	0.9793
Resolution (Å)	47.02–3.34
Space group	$P2_12_12_1$
Unit-cell parameters (Å)	a = 73.9, b = 88.2, c = 421.6
Molecules in asymmetric unit	4
R_{meas}†	0.08 (0.30)
No. of observations	287508
No. of unique reflections	40578
Completeness (%)	98.3 (82.0)
Multiplicity	7.0 (5.4)
Mean $I/\sigma(I)$‡	13.4 (2.5)
No. of Se sites	20
Figure of merit	0.28
Residues in model	*A*(−5)–*A*430, *B*1–*B*430, *C*4–*C*430, *D*4–*D*430
R_{cryst}§	0.207
R_{free}§	0.248
Wilson *B* factors (Å^2)	55.5
R.m.s deviations from ideal geometry	
Bond lengths (Å)	0.009
Bond angles (°)	1.261
Ramachandran plot statistics (%)	
Favoured	93.7
Allowed	99.8
Disallowed	0.2

† As defined by Diederichs & Karplus (1997). ‡ Mean $I/\sigma(I)$ indicates the average of the intensity divided by its standard deviation. § $R_{cryst} = \sum_{hkl} ||F_{obs}| - |F_{calc}|| / \sum_{hkl} |F_{obs}|$, where F_{obs} and F_{calc} are the observed and calculated structure-factor amplitudes, respectively. R_{free} was calculated from a randomly chosen 5% of all unique reflections.

Ent *et al.*, 2001), and has therefore been suggested to primarily function in cell-shape determination (Ettema *et al.*, 2011). In accordance, the presence of the *cren*-1 gene encoding crenactin is strongly correlated with elongated cell morphologies within Crenarchaeota, as well as in the candidate phylum Korarchaeota (Ettema *et al.*, 2011).

The *cren*-1 gene belongs to a conserved five-gene operon within Thermoproteales denoted Arcade (**a**ctin-**r**elated **c**ytoskeleton in **a**rchaea involved in shape **de**termination (Ettema *et al.*, 2011). Three of the four arcadin proteins show spiral-shaped patterns in immunostained *P. calidifontis* cells and are therefore likely to interact with crenactin filaments (Ettema *et al.*, 2011). In contrast, the arcadin 2 protein shows a punctuated intracellular distribution compatible with a function in genome segregation or cell division (Ettema *et al.*, 2011).

The crystal structures of a large number of eukaryotic actins have been reported (see, for example, Kabsch *et al.*, 1990; Vorobiev *et al.*, 2003; Otterbein *et al.*, 2001), as well as that of MreB from the hyperthermophilic bacterium *Thermotoga maritima* (van den Ent *et al.*, 2001). Eukaryotic actin (Fig. 1*b*) and MreB (Fig. 1*c*) share the same basic three-dimensional core, although the details vary. The proteins contain two major domains, I and II, between which a deep cleft provides binding sites for ATP and a divalent metal ion (Mg^{2+} or Ca^{2+}). Each of the main domains is in turn divided into two subdomains (Ia, Ib, IIa and IIb; Fig. 1*a*). Subdomains Ia and IIa both contain a five-stranded β-sheet structure with flanking α-helices that is a characteristic feature of actin-family proteins. A range of alternative actin structures have also been described depending on, for example, the particular actin isomer and the presence of specific associated ABPs or actin-binding antibiotics and other drugs (Dominguez & Holmes, 2011).

Here, we present the three-dimensional structure of ADP-bound crenactin at 3.35 Å resolution and describe a helical structure in the crystal. Comparisons with actin and MreB add to the understanding of the structural and functional properties of the actin superfamily and provide insights into the evolutionary trajectory that gave rise to present-day actins.

2. Materials and methods

2.1. Cloning and expression

The *cren*-1 (*pcal_1635*) gene was previously amplified (Ettema *et al.*, 2011) using PCR and cloned into the pET-45b(+) expression vector (Novagen). Recombinant crenactin with an N-terminal histidine tag was overexpressed in *Escherichia coli* strain Rosetta DE3. Native crenactin was produced as described in Lindås *et al.* (2008) and selenomethionine-substituted (SeMet) crenactin was produced using a metabolic inhibition protocol as described below.

Cells were grown overnight at 37°C in 2 ml 2×YT medium containing ampicillin at 50 µg ml^{-1}. The starter culture was used to inoculate 50 ml M9 minimal medium (50 m*M* Na_2HPO_4, 3 g l^{-1} KH_2PO_4, 0.5 g l^{-1} NaCl, 1 g l^{-1} NH_4Cl) and the culture was grown at 37°C until an OD_{600} of 0.5 was reached. An aliquot (50 ml) was added to 700 ml M9 medium supplemented with 2 m*M* $MgSO_4$, 0.1 m*M* $CaCl_2$, 0.4% glucose and 50 µg ml^{-1} ampicillin. The cells were grown at 37°C until an OD_{600} of 0.4–0.6 was reached, after which the following L-amino acids were added: Lys, Phe and Tyr (100 mg l^{-1}), Leu, Ile and Thr (50 mg l^{-1}) and L-selenomethionine (Acros Organics; final concentration of 60 mg l^{-1}). When the culture reached an OD_{600} of 0.6–0.8, expression of the native protein was induced by the addition of 0.5 m*M* IPTG (isopropyl β-D-1-thiogalactopyranodside) followed by overnight incubation.

2.2. Purification and crystallization

The bacterial cells were harvested by centrifugation at 10 000*g*, resuspended in 0.02 *M* sodium phosphate buffer pH 7.5, 0.5 *M* NaCl, 2 m*M* $MgCl_2$, Benzonase nuclease (Novagen) and one complete protease-inhibitor tablet (Roche). Cell lysis was performed using a One Shot cell disruptor (Constant Cell Disruptor Systems) and the lysate was cleared by centrifugation at 20 000*g*. The supernatant was applied onto a HiTrap Chelating HP column (GE Healthcare) loaded with Ni^{2+}. The column was washed with 0.05 *M* imidazole, 0.02 *M* sodium phosphate buffer pH 7.5, 0.5 *M* NaCl before elution of crenactin using a gradient of 0.05–0.5 *M* imidazole in 0.02 *M* sodium phosphate buffer pH 7.5, 0.5 *M* NaCl. The crenactin fractions were pooled and the buffer was changed to 0.025 *M* Tris–HCl pH 7.5, 0.1 *M* NaCl using a Vivaspin 10 000 MWCO concentrator (Vivascience).

Crystallization experiments were performed at 20°C using the hanging-drop vapour-diffusion method. Both native and SeMet-derivative crystals were obtained after mixing equal volumes of protein solution (1.2 mg ml^{-1}) and reservoir solution consisting of 4.5%(*w*/*v*) polyethylene glycol 6000, 0.1 *M* NaCl, 0.1 *M* MES buffer pH 6. The droplets were equilibrated against the reservoir solution. Needle-shaped crystals appeared after 3–6 weeks. Prior to data collection, crystals were transferred into a cryosolution consisting of 20%(*w*/*v*) glycerol, 10%(*w*/*v*) polyethylene glycol 6000, 0.1 *M* NaCl, 0.1 *M* MES buffer pH 6 and flash-cooled in liquid nitrogen.

2.3. Data collection and structure determination

The structure of crenactin was determined to 3.35 Å resolution using the single-wavelength anomalous dispersion (SAD) method with selenomethionine-substituted protein, Data were collected at 100 K on beamline ID29 at the ESRF, Grenoble. Structure determination was performed using *HKL*-3000 (Minor *et al.*, 2006). *HKL*-3000 is integrated with *SHELXC*/*D*/*E* (Sheldrick, 2008), *MLPHARE* (Otwinowski, 1991), *DM* (Cowtan & Main, 1993), *Buccaneer* (Cowtan, 2006), *CCP*4 (Winn *et al.*, 2011), *SOLVE* and *RESOLVE* (Terwilliger, 2004). The model was improved by manual rebuilding in *Coot* (Emsley & Cowtan, 2004) and *O* (Jones *et al.*, 1991). Several data sets were collected from native crystals. All of these data sets showed a high degree of anisotropy, and therefore the high-quality SeMet data were used to refine the structure. Refinement was performed using the programs *HKL*-3000 (Minor *et al.*, 2006), *REFMAC*5 (Murshudov *et al.*, 2011) and *BUSTER* (Smart *et al.*, 2012). The final statistics of data collection and structural refinement are shown in Table 1. Figures were prepared in *PyMOL* (http://pymol.org/).

3. Results

3.1. Overall structure of crenactin

Crystallographic studies of crenactin from *P. calidifontis* were initiated in order to obtain insights into the structural and functional characteristics of a heat-stable archaeal actin and to generate data for comparative investigations of actin-family members from all three domains of life.

Crenactin crystallized in the orthorhombic space group $P2_12_12_1$, with unit-cell parameters $a = 73.9$, $b = 88.2$, $c = 421.6$ Å (Table 1). The asymmetric unit contains four protein monomers (V_M = 3.5 Å^3 Da^{-1}), corresponding to a crystal solvent content of 65%(*v*/*v*). The structure was determined to 3.35 Å resolution by the SAD method using selenomethionine-substituted protein.

The overall structure of crenactin clearly confirms its membership of the actin superfamily. Thus, although the sequence identity is below 20% and although the archaeal actin is longer than *Saccharomyces cerevisiae* actin and *T. maritima* MreB (452, 375 and 344 amino acids for crenactin, *S. cerevisiae* actin and MreB, respectively), their three-dimensional structures are still highly similar (Fig. 1). Several highly conserved regions are consequently evident in the monomer structures, as described in detail below, with individual conserved residues preferentially located around the active site and along the inward surface of subdomains Ib and IIb.

The three-dimensional structure is a heart-shaped molecule with dimensions of 56 × 56 × 38 Å (Fig. 1*a*). Similar to actin (Fig. 1*b*) and MreB (Fig. 1*c*), the structure contains two major domains, I and II, between which

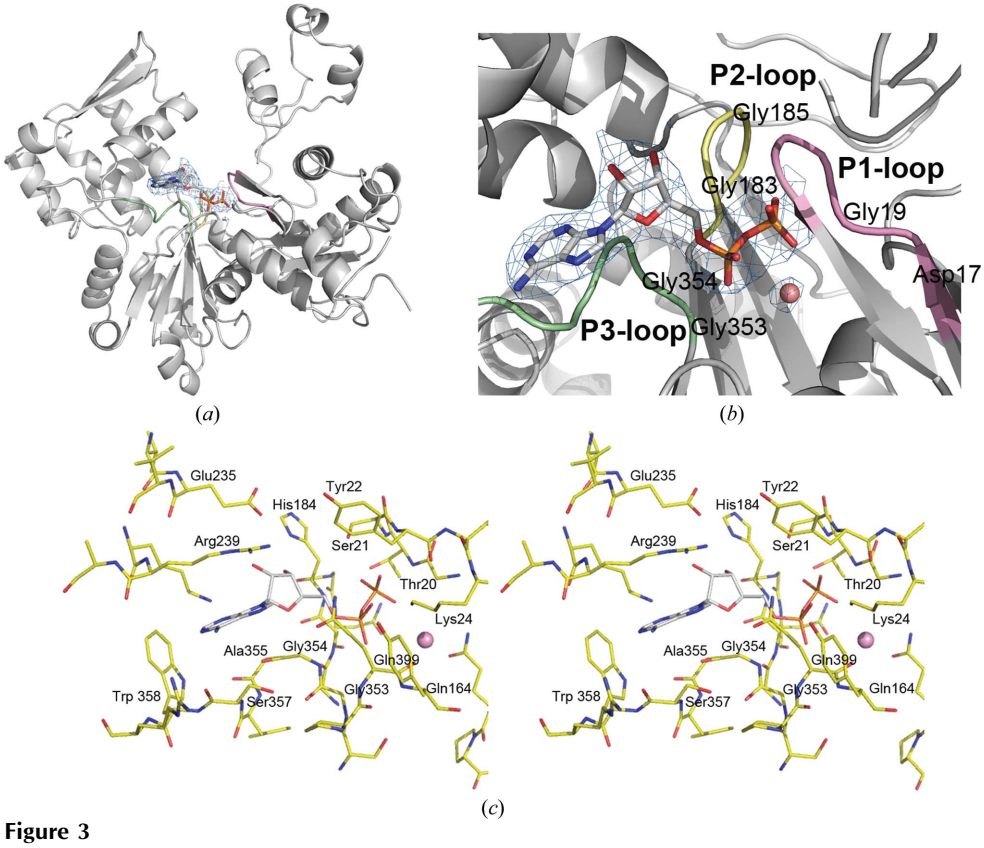

Figure 3
Crystal structure of the crenactin–ADP complex. (*a*) ADP nucleotide and divalent metal ion bound at the base of the cleft between domains I and II. (*b*) Close-up showing the $2F_o - F_c$ electron-density map contoured at 1σ around the ADP and the metal ion. The three highly conserved P-loops are indicated in pink (P1), yellow (P2) and green (P3). The P-loops are also indicated in the sequence alignment in Fig. 2. A selection of conserved amino-acid residues that interact with the nucleotide are also indicated. (*c*) Stereoview of the active site, showing the residues which interact with ADP.

a deep cleft forms the binding site for the nucleotide and a divalent metal ion. Also similar to the other two actin-family members, the two domains can be further subdivided into two smaller domains each (Fig. 1*a*), consisting of residues 1–38, 90–164 and 397–430 (subdomain Ia), residues 39–89 (subdomain Ib), residues 165–207 and 288–396 (subdomain IIa) and residues 208–287 (subdomain IIb). [The alternative I, II, III, IV nomenclature is also in use (Kabsch *et al.*, 1990)]. Subdomains Ia and IIa, which may have arisen through an ancient gene duplication (Kabsch *et al.*, 1990), fold into five-stranded β-sheets with flanking α-helices whose conformation is highly similar to the corresponding domains in actin and MreB (Fig. 2). The two smaller subdomains, Ib and IIb, are more variable in size and structure. Subdomain Ib of crenactin contains three short helices, while in yeast actin and MreB a single β-sheet together with one α-helix are evident. The N- and C-termini of the protein are both located in subdomain Ia in all three actin-family members.

Four major differences are apparent in crenactin compared with yeast actin and MreB (Figs. 1 and 2). The largest of these is an insertion (residues 293–325) in the long α-helix domain connecting subdomains IIa and IIb (designated 1 in Fig. 1*d* and Fig. 2). The domain is denoted the 'hydrophobic plug' in eukaryotic actin (Figs. 1*e* and 2) and has been proposed to mediate association between the polymers in F-actin (Holmes *et al.*, 1990; Chen *et al.*, 1993). The domain is absent in MreB (Fig. 1*f*). An insertion (residues 45–62) at the top of subdomain Ib (designated 2 in Figs. 1*a* and 2) folds into two short α-helices and is involved in the interaction with the next monomer in the crenactin filament (below). A similar loop is evident in yeast actin (Fig. 1*b*) but is missing in MreB (Fig. 1*c*). A third difference is an extra loop (residues 358–370) that is not present in yeast actin and MreB (designated 3 in Figs. 1*a* and 2). Finally, the C-terminus of crenactin (designated 4 in Figs. 1*a* and 2) folds into a structure that differs from those of both actin and MreB.

3.2. Nucleotide and metal ion binding pocket

Although no nucleotides were exogenously added to the crystallization buffer, an ADP molecule, presumably originating from the expression host, was readily identified in the active site in three of the four monomers in the asymmetric unit. The nucleotide binds at the base of the cleft formed by domains I and II (Fig. 3*a*), and electron density for a divalent metal ion (Mg^{2+} or Ca^{2+}) was resolved in the active site in one of the monomers.

As expected, the residues that interact with the nucleotide are well conserved in crenactin (Fig. 3). Similar to yeast actin and MreB, crenactin contains three highly conserved P-loops (phosphate-binding loops), corresponding to residues 16–21 (P1), 179–192 (P2) and 349–355 (P3), which are responsible for recognizing the nucleotide. The purine base binds in a hydrophobic pocket formed by the side chains of Gly353, Gly354, Ala355, Trp358 and Arg239, in which the adenine ring makes stacking interactions with Arg239 and the (N6) amino group is hydrogen-bonded to the backbone carbonyl O atom of Ser357. The ribose O atoms participate in specific interactions with the 3′-oxygen hydrogen-bonded to the side chain of His184 from the P2-loop, and the 2′-oxygen interacts with the side chain of Glu235. In addition, the phosphates of the ADP form numerous contacts with the protein. One of the α-phosphoryl O atoms interacts with the side chains of Lys24 and Gln399. The nonbridging β-phosphoryl O atoms participate in hydrogen bonding to the backbone amide N atom and the side chain of Ser21, the backbone amide N atom of Tyr22, the conserved side chain of Lys24 and the backbone amide N atom of Thr20 (P1-loop). A conserved residue in the active site, Gln164, has been proposed to activate the nucleophile, a water molecule, which attacks the γ-phosphate of ATP (Vorobiev *et al.*, 2003).

The superposition of crenactin with yeast actin (Fig. 4*a*) and with *T. maritima* MreB (Fig. 4*b*) further underscores the striking similarities in active-site architecture, as well as the high conservation of the residues that line the nucleotide-binding pocket. This is exemplified by the two conserved glycins, Gly353 and Gly354, in the active site which reside close to the ribose and the polyphosphate tail in all three proteins, as well as by a helix (residues 400–412) that

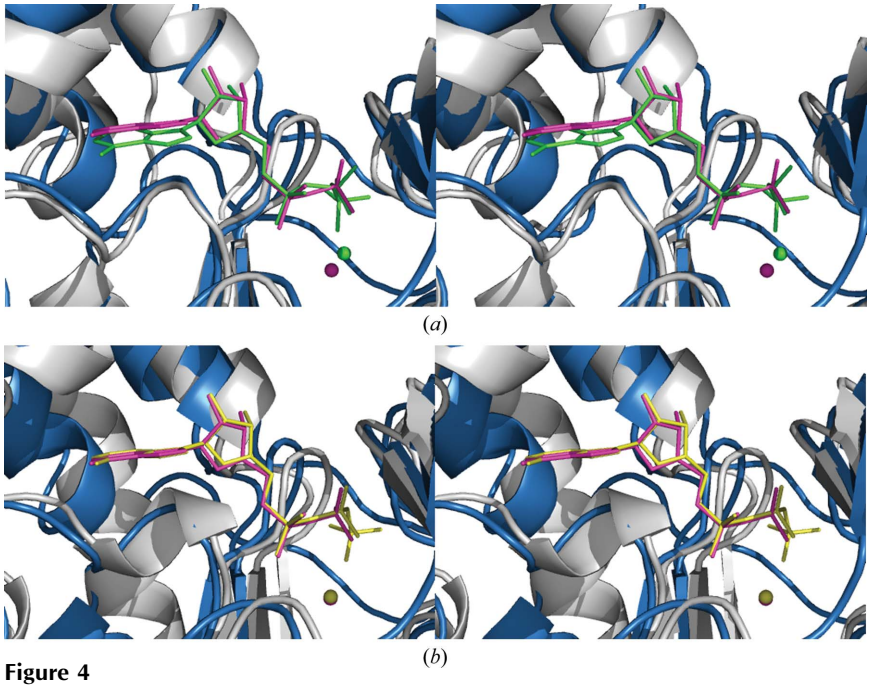

Figure 4
Comparison of nucleotide and metal ion binding pocket. (*a*) Stereoview of superposition of crenactin from *P. calidifontis* (blue) and yeast actin from *S. cerevisiae* (PDB entry 1yag; grey). (*b*) Stereoview of superposition of crenactin (blue) and MreB from *T. maritima* (PDB entry 1jcg; grey). Bound nucleotides and metal ions are shown in magenta for crenactin (ADP, Mg^{2+}), green for yeast actin (ATP, Mg^{2+}) and yellow for MreB (AMP-PNP, Mg^{2+}).

may contribute to stabilization of the nucleotide-binding site (Figs. 2 and 3).

3.3. Antibiotic-interaction sites

The antibiotic A22 [*S*-(3,4-dichlorobenzyl)isothiourea] interferes with MreB polymerization in *T. maritima* through competitive inhibition of ATP binding (Bean *et al.*, 2009). No significant effects of A22 on the growth of *P. calidifontis* cultures, or on the polymerization of crenactin, are evident *in vivo* (Ettema *et al.*, 2011). However, inhibition of crenactin-mediated ATP hydrolysis is observed *in vitro* (Ettema *et al.*, 2011) at 50°C, although at a significantly higher A22 concentration compared with MreB. Docking studies show that the main interaction of A22 with MreB occurs through residues Glu131, Thr158 and Val315 (Bean *et al.*, 2009), corresponding to positions Gln164, Asn186 and Val402 in crenactin (Fig. 2). Glu131 and Thr158 are conserved in the bacterial MreB family (van den Ent *et al.*, 2001), and the substitutions at these positions in crenactin (and actin) may contribute to the reduced binding and decreased inhibitory effects of A22.

Cytochalasins are fungal metabolites that bind to the (+)-end of actin and prevent polymerization without affecting ATP hydrolysis (Cooper, 1987). Neither cytochalasins B nor D affect the growth of *P. calidifontis* cultures, the *in vivo* polymerization of crenactin or ATP hydrolysis *in vitro* (Ettema *et al.*, 2011). The hydrophobic cleft between subdomains Ia and IIa constitutes the major binding site for cytochalasins (Nair *et al.*, 2008; Dominguez & Holmes, 2011). The crystal structure of *Drosophila* 5C cytoplasmic actin in complex with cytochalasin D shows that residues Ile136, Tyr169, Ala170, Pro172, Met355 and Phe375 confer major contacts with cytochalasins (Nair *et al.*, 2008). The amino-acid sequence of the corresponding binding cleft in crenactin is not conserved, in agreement with its resistance to cytochalasins B and D.

3.4. Filament structure

The crenactin monomers assembled into right-handed helical filaments in the crystals (Figs. 5*a* and 5*b*). The monomers interact head-to-tail with a longitudinal subunit spacing of 53 Å, which is intermediate between the monomer repeat distances of yeast actin (55 Å) and MreB (51 Å). Eight crenactin monomers form a full turn of the helix in the

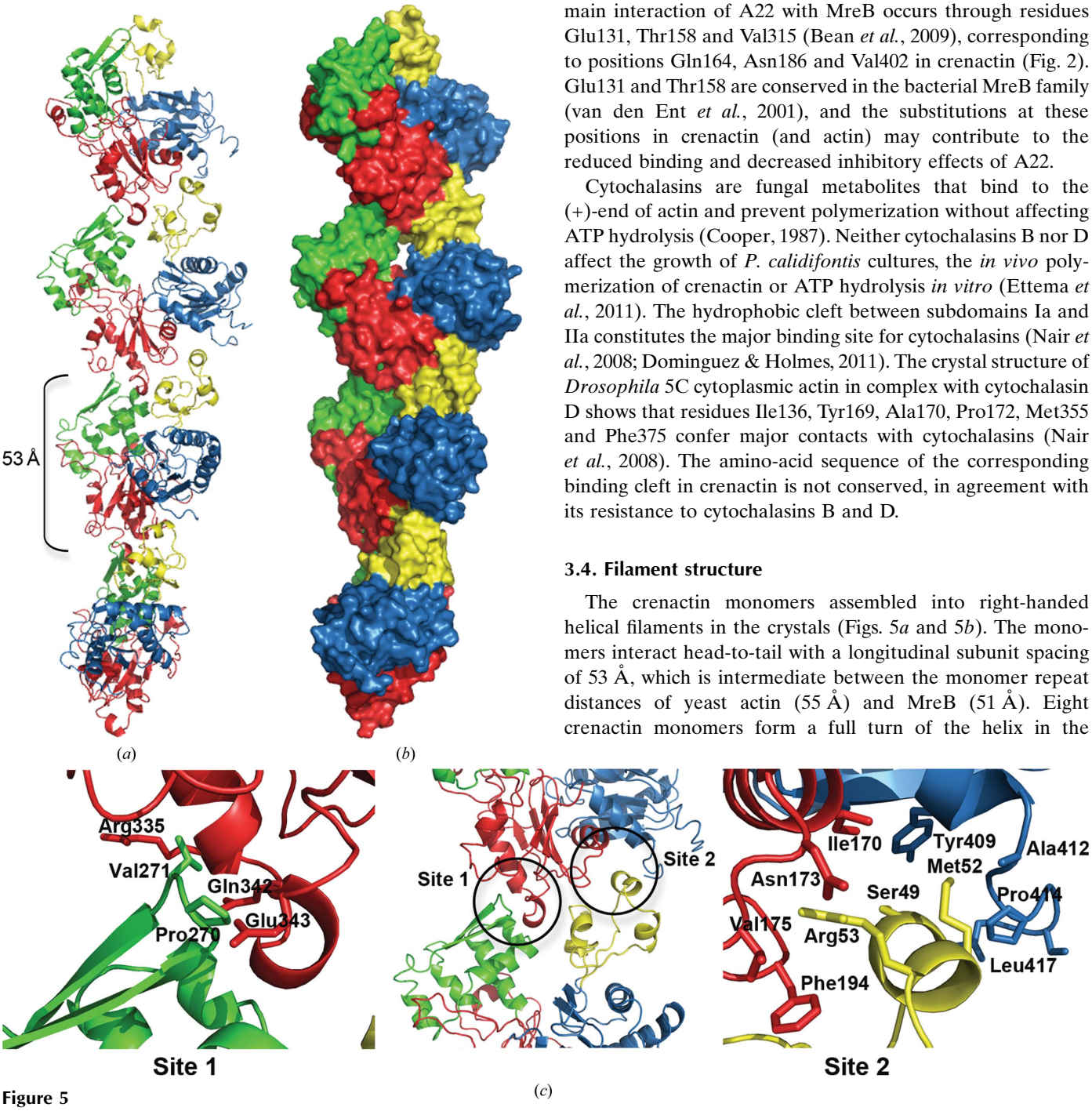

Figure 5
Structure of the crenactin polymer. The protein monomers assemble into a right-handed helical filament in the crystals. (*a*) Ribbon representation containing four crenactin monomers. The four subdomains are coloured blue (subdomain Ia), yellow (Ib), red (IIa) and green (IIb). The (−)-end of the filament is at the top and the (+)-end at the bottom. (*b*) Surface model. Subdomains are coloured as in (*a*). (*c*) Close-up of the monomer interface. The two main monomer–monomer interaction sites are indicated in the middle panel. Site 1 (left panel) consists of a short helix (residues Val339–Gln342) in subdomain IIa interacting with a loop (Ser269–Val272) in subdomain IIb in the next monomer. Site 2 (right panel) consists of a short helix (Glu48–Met52) in subdomain Ib that interacts with residues in subdomains Ia and IIa in the next monomer. Note the position of the Met52 residue, which in eukaryotes (Met44) is implicated in oxidation-mediated regulation of filament disassembly (see text for details).

crystals, with a repeat distance of 421.6 Å (crystallographic *c* axis). The helix-forming ability of crenactin agrees well with its capacity to form intracellular spiral-shaped cytoskeletal structures *in vivo* (Ettema *et al.*, 2011), as well as with the filament-forming properties of both eukaryotic actin and bacterial MreB (Dominguez & Holmes, 2011; van den Ent *et al.*, 2001).

Two main subunit-interaction sites are evident in the crenactin filament (Fig. 5*c*). Site 1 is formed by a short helix (residues Val339–Gln342) in subdomain IIa that interacts with a loop (Ser269–Val272) in subdomain IIb in the next monomer in the filament. At site 2, a short helix (Glu48–Met52) in subdomain IIb interacts with residues in both subdomains IIa and Ia in the next monomer.

Two conserved methionine residues, Met44 and Met47, situated in the so-called D-loop (DNase I binding loop) of actin provide targets for MICAL, a multidomain monooxygenase which oxidizes these to methionine sulfoxide in response to extracellular cues mediated through the semaphorin signalling pathway (Hung *et al.*, 2011). The modification of Met44 causes the depolymerization of F-actin (Hung *et al.*, 2011). The modifications are reversed by the action of methionine sulfoxide reductases (MSRs), which thus work in concert with MICAL to regulate actin dynamics (Lee *et al.*, 2013). Interestingly, the Met44 residue is conserved in crenactin (Met52) and is conspicuously located at the monomer interface in the polymer (Figs. 2 and 5*c*). This conservation is particularly striking in light of the highly oxidative conditions that characterize the extreme growth environment of the aerobic hyperthermophile *P. calidifontis*, which should provide strong selection against retaining a residue prone to oxidation at this position. Although homologues of MICAL and MSRs remain to be identified in *P. calidifontis*, it is therefore tempting to speculate that the preservation of Met52 may result from the conservation of a mechanism that regulates crenactin polymerization by affecting the oxidation state of this residue.

4. Discussion

We report the crystal structure of crenactin, the first cytoskeletal protein identified in archaea and the first actin to be active at 90°C. Similar to other archaeal molecular and cellular features, for example the transcriptional and translational machineries (Olsen & Woese, 1997; Bernander, 2000), crenactin and the cytoskeleton display a combination of properties considered to be characteristic of either eukaryotes or bacteria. Thus, at both the protein-sequence and structural levels crenactin is most similar to eukaryotic actin, while at the functional level the protein forms spiral-shaped structures implicated in shape determination, similar to bacterial MreB.

The overall structure of the crenactin monomer is highly similar to those of eukaryotic and bacterial actin-family members. This is particularly pronounced in the active-site region, which closely resembles those of yeast actin and MreB, including the nucleotide-binding pocket, P-loops and the adjacent divalent metal ion. Furthermore, crenactin has been shown to hydrolyze ATP (Ettema *et al.*, 2011) and ADP, presumably originating from the expression host in the form of ATP bound to purified monomers, co-crystallized with the protein. Together, this suggests that nucleotide-binding characteristics and interaction details, as well as the catalytic mechanism that mediates ATP hydrolysis, have been conserved in all three protein families despite the immense evolutionary distances. In addition, the differential antibiotic susceptibility of crenactin, actin and MreB correlated well with substitutions of residues known to be involved in drug interaction.

In the crenactin crystals the monomers interacted head-to-tail, forming a helical filament structure, as previously observed for both actin and MreB (van der Ent *et al.*, 2001; Holmes *et al.*, 1990; Fujii *et al.*, 2010; Otterbein *et al.*, 2001). Elucidation of the extent to which this represents the *in vivo* structure will require additional work, although we note that models currently regarded as likely to accurately reflect the *in vivo* structure of F-actin are incompatible with crystal formation (Reisler & Egelman, 2007). It is therefore possible that intracellular crenactin filaments may differ in, for example, the number of subunits per full turn and pitch per monomer compared with the crystal form. The specific amino-acid residues and surfaces involved in monomer–monomer interactions in the crystal are still likely to reflect true interactions *in vivo*, although the atomic distances and bond angles may differ slightly. In addition, the structure will serve as a basis for predictions about possible protein-binding surfaces, *e.g.* for the arcadins (see §1), and for selection of target residues for site-directed mutagenesis aimed at detailed investigation of such interactions.

In light of the extensive similarities at both the monomer and filament levels, we propose that the molecular mechanisms of crenactin polymerization and depolymerization resemble those of actin. We predict that monomers initially associate at the (+)-end of the crenactin filament in the ATP-bound form, that subsequent hydrolysis to ADP within the filament contributes to stabilization of the polymer and that ADP-bound monomers are eventually released. We also speculate that the conservation of the methionine residue Met52 at the monomer interface is indicative of the preservation of an oxidation-mediated mechanism for regulation of filament disassembly, as in eukaryotic actin. Furthermore, it is likely that the brightly fluorescing helical-shaped structures observed in immunostained *P. calidifontis* cells (Ettema *et al.*, 2011) consist of bundles of crenactin polymers. It remains to be determined whether such putative bundling might involve an F-actin-like crenactin structure and whether it might be mediated by the hydrophobic plug-like domain.

In terms of functional roles, the spiral-shaped intracellular crenactin structures, as well as the close coupling between elongated cell morphologies and presence of the *cren*-1 gene in Thermoproteales (Ettema *et al.*, 2011), suggest that the primary role of crenactin concerns cell-shape determination. In bacteria, MreB spirals have been suggested to interact with the peptidoglycan-biosynthesis machinery and slowly rotate inside the cell along with the incorporation of new cell-wall

material (Domínguez-Escobar *et al.*, 2011; van Teeffelen *et al.*, 2011). Since the *P. calidifontis* cell surface is covered with a proteinaceous S (surface) layer, rather than peptidoglycan, the molecular details of a molecular coupling between crenactin spirals and the S-layer synthesis machinery would be expected to be different compared with MreB. Furthermore, MreB has been shown to form ring-shaped structures in association with the bacterial FtsZ cell-division protein (Vats *et al.*, 2009). A role for crenactin in the cell-division process, possibly in conjunction with one or several of the arcadin proteins, is therefore also possible. Further investigations into the molecular and structural properties of crenactin and the arcadins will aid in elucidation of their roles in shape determination, S-layer synthesis and cell division.

The determination of the molecular structure of the first cytoskeletal element from an archaeon provides a basis for further comparative studies of the structural and functional characteristics of actin-family members in all three domains of life. This is essential for our understanding of the evolutionary history of the actin protein family, including the events that gave rise to the eukaryotic actin cytoskeleton and perhaps even the eukaryotic cell itself (Yutin *et al.*, 2009; Bernander *et al.*, 2011).

This work was supported by grant 621-2010-5551 from the Swedish Research Council to RB. We are grateful to Robert M. Sweet, Roger Karlsson and Rodney Levine for valuable discussions. The European Synchrotron Research Facility is acknowledged for beam time and assistance.

References

Amo, T., Paje, M. L. F., Inagaki, A., Ezaki, S., Atomi, H. & Imanaka, T. (2002). *Archaea*, **1**, 113–121.

Bean, G. J., Flickinger, S. T., Westler, W. M., McCully, M. E., Sept, D., Weibel, D. B. & Amann, K. J. (2009). *Biochemistry*, **48**, 4852–4857.

Bernander, R. (2000). *Trends Microbiol.* **8**, 278–283.

Bernander, R., Lind, A. E. & Ettema, T. J. G. (2011). *Commun. Integr. Biol.* **4**, 664–667.

Bork, P., Sander, C. & Valencia, A. (1992). *Proc. Natl Acad. Sci. USA*, **89**, 7290–7294.

Carballido-López, R. (2006). *Microbiol. Mol. Biol. Rev.* **70**, 888–909.

Chen, X., Cook, R. K. & Rubenstein, P. A. (1993). *J. Cell Biol.* **123**, 1185–1195.

Cooper, J. A. (1987). *J. Cell Biol.* **105**, 1473–1478.

Cowtan, K. (2006). *Acta Cryst.* D**62**, 1002–1011.

Cowtan, K. D. & Main, P. (1993). *Acta Cryst.* D**49**, 148–157.

Derman, A. I., Becker, E. C., Truong, B. D., Fujioka, A., Tucey, T. M., Erb, M. L., Patterson, P. C. & Pogliano, J. (2009). *Mol. Microbiol.* **73**, 534–552.

Diederichs, K. & Karplus, P. A. (1997). *Nature Struct. Biol.* **4**, 269–275.

Dominguez, R. & Holmes, K. C. (2011). *Annu. Rev. Biophys.* **40**, 169–186.

Domínguez-Escobar, J., Chastanet, A., Crevenna, A. H., Fromion, V., Wedlich-Söldner, R. & Carballido-López, R. (2011). *Science*, **333**, 225–228.

Emsley, P. & Cowtan, K. (2004). *Acta Cryst.* D**60**, 2126–2132.

Ent, F. van den, Amos, L. A. & Löwe, J. (2001). *Nature (London)*, **413**, 39–44.

Ent, F. van den, Møller-Jensen, J., Amos, L. A., Gerdes, K. & Löwe, J. (2002). *EMBO J.* **21**, 6935–6943.

Ettema, T. J. G., Lindås, A.-C. & Bernander, R. (2011). *Mol. Microbiol.* **80**, 1052–1061.

Fujii, T., Iwane, A. H., Yanagida, T. & Namba, K. (2010). *Nature (London)*, **467**, 724–728.

Goodson, H. V. & Hawse, W. F. (2002). *J. Cell Sci.* **115**, 2619–2622.

Holm, L. & Rosenström, P. (2010). *Nucleic Acids Res.* **38**, 545–549.

Holmes, K. C., Popp, D., Gebhard, W. & Kabsch, W. (1990). *Nature (London)*, **347**, 44–49.

Hung, R.-J., Pak, C. W. & Terman, J. R. (2011). *Science*, **334**, 1710–1713.

Jones, L. J. F., Carballido-López, R. & Errington, J. (2001). *Cell*, **104**, 913–922.

Jones, T. A., Zou, J.-Y., Cowan, S. W. & Kjeldgaard, M. (1991). *Acta Cryst.* A**47**, 110–119.

Kabsch, W., Mannherz, H. G., Suck, D., Pai, E. F. & Holmes, K. C. (1990). *Nature (London)*, **347**, 37–44.

Komeili, A., Li, Z., Newman, D. K. & Jensen, G. J. (2006). *Science*, **311**, 242–245.

Lee, B. C., Péterfi, Z., Hoffmann, F. W., Moore, R. E., Kaya, A., Avanesov, A., Tarrago, L., Zhou, Y., Weerapana, E., Fomenko, D. E., Hoffmann, P. R. & Gladyshev, V. N. (2013). *Mol. Cell*, **51**, 397–404.

Lindås, A.-C., Karlsson, E. A., Lindgren, M. T., Ettema, T. J. G. & Bernander, R. (2008). *Proc. Natl Acad. Sci. USA*, **105**, 18942–18946.

Minor, W., Cymborowski, M., Otwinowski, Z. & Chruszcz, M. (2006). *Acta Cryst.* D**62**, 859–866.

Murshudov, G. N., Skubák, P., Lebedev, A. A., Pannu, N. S., Steiner, R. A., Nicholls, R. A., Winn, M. D., Long, F. & Vagin, A. A. (2011). *Acta Cryst.* D**67**, 355–367.

Nair, U. B., Joel, P. B., Wan, Q., Lowey, S., Rould, M. A. & Trybus, K. M. (2008). *J. Mol. Biol.* **384**, 848–864.

Olsen, G. J. & Woese, C. R. (1997). *Cell*, **89**, 991–994.

Otterbein, L. R., Graceffa, P. & Dominguez, R. (2001). *Science*, **293**, 708–711.

Otwinowski, Z. (1991). *Proceedings of the CCP4 Study Weekend. Isomorphous Replacement and Anomalous Scattering*, edited by W. Wolf, P. R. Evans & A. G. W. Leslie, pp. 80–87. Warrington: Daresbury Laboratory.

Pollard, T. D. & Cooper, J. A. (2009). *Science*, **326**, 1208–1212.

Reisler, E. & Egelman, E. H. (2007). *J. Biol. Chem.* **282**, 36133–36137.

Remedios, C. G. dos, Chhabra, D., Kekic, M., Dedova, I. V., Tsubakihara, M., Berry, D. A. & Nosworthy, N. J. (2003). *Physiol. Rev.* **83**, 433–473.

Roeben, A., Kofler, C., Nagy, I., Nickell, S., Hartl, F. U. & Bracher, A. (2006). *J. Mol. Biol.* **358**, 145–156.

Schafer, D. A. & Schroer, T. A. (1999). *Annu. Rev. Cell Dev. Biol.* **15**, 341–363.

Sheldrick, G. M. (2008). *Acta Cryst.* A**64**, 112–122.

Smart, O. S., Womack, T. O., Flensburg, C., Keller, P., Paciorek, W., Sharff, A., Vonrhein, C. & Bricogne, G. (2012). *Acta Cryst.* D**68**, 368–380.

Teeffelen, S. van, Wang, S., Furchtgott, L., Huang, K. C., Wingreen, N. S., Shaevitz, J. W. & Gitai, Z. (2011). *Proc. Natl Acad. Sci. USA*, **108**, 15822–15827.

Terwilliger, T. (2004). *J. Synchrotron Rad.* **11**, 49–52.

Vats, P., Yu, J. & Rothfield, L. (2009). *Cell. Mol. Life Sci.* **66**, 3353–3362.

Vorobiev, S., Strokopytov, B., Drubin, D. G., Frieden, C., Ono, S., Condeelis, J., Rubenstein, P. A. & Almo, S. C. (2003). *Proc. Natl Acad. Sci. USA*, **100**, 5760–5765.

Winn, M. D. *et al.* (2011). *Acta Cryst.* D**67**, 235–242.

Yutin, N., Wolf, M. Y., Wolf, Y. I. & Koonin, E. V. (2009). *Biol. Direct*, **4**, 9.